

Preparation and properties of GAGG:Ce/glass composite scintillation material

Wei-Jie Zhang(张伟杰), Qin-Hua Wei(魏钦华), Xiao Shen(沈潇), Gao Tang(唐高), Zhen-Hua Chen(陈振华), Lai-Shun Qin(秦来顺), and Hong-Sheng Shi(史宏声)

Citation: Chin. Phys. B, 2021, 30 (**7**): 074205. DOI: 10.1088/1674-1056/abe3ea
Journal homepage: http://cpb.iphy.ac.cn; http://iopscience.iop.org/cpb

What follows is a list of articles you may be interested in

An ultrafast and low-power slow light tuning mechanism for compact aperture-coupled disk resonators

Bo-Yun Wang(王波云), Yue-Hong Zhu(朱月红), Jing Zhang(张静), Qing-Dong Zeng(曾庆栋), Jun Du(杜君), Tao Wang(王涛), Hua-Qing Yu(余华清)

Chin. Phys. B, 2020, 29 (**8**): 084211. DOI: 10.1088/1674-1056/ab9df1

Preparation and characterization of nanosized $Gd_xBi_{0.95-x}VO_4$：$0.05Eu^{3+}$ solid solution as red phosphor

Yi Juan, Qiu Jian-Bei, Wang Yu-An, Zhou Da-Cheng

Chin. Phys. B, 2014, 23 (**10**): 104224. DOI: 10.1088/1674-1056/23/10/104224

Green long-after-glow luminescence of Tb^{3+} in Sr_2SiO_4

Wang Qi, Qiu Jian-Bei, Song Zhi-Guo, Zhou Da-Cheng, Xu Xu-Hui

Chin. Phys. B, 2014, 23 (**6**): 064211. DOI: 10.1088/1674-1056/23/6/064211

Spectroscopic properties and mechanism of $Tm^{3+}/Er^{3+}/Yb^{3+}$ co-doped oxyfluorogermanate glass ceramics containing BaF_2 nanocrystals

Hu Yue-Bo, Qiu Jian-Bei, Zhou Da-Cheng, Song Zhi-Guo, Yang Zheng-Wen, Wang Rong-Fei, Jiao Qing, Zhou Da-Li

Chin. Phys. B, 2014, 23 (**2**): 024205. DOI: 10.1088/1674-1056/23/2/024205

Microstructure and optical properties of nitrogen-doped ZnO film

Zhao Xian-Wei, Gao Xiao-Yong, Chen Xian-Mei, Chen Chao, Zhao Meng-Ke

Chin. Phys. B, 2013, 22 (**2**): 024202. DOI: 10.1088/1674-1056/22/2/024202

Preparation and properties of GAGG:Ce/glass composite scintillation material*

Wei-Jie Zhang(张伟杰)[1], Qin-Hua Wei(魏钦华)[1,†], Xiao Shen(沈潇)[1], Gao Tang(唐高)[1], Zhen-Hua Chen(陈振华)[1], Lai-Shun Qin(秦来顺)[1], and Hong-Sheng Shi(史宏声)[2,‡]

[1] *College of Materials and Chemistry, China Jiliang University, Hangzhou* 310018, *China*
[2] *Xinjiang Technical Institute of Physics & Chemistry, Chinese Academy of Sciences, Urumqi* 830011, *China*

(Received 2 December 2020; revised manuscript received 2 February 2021; accepted manuscript online 7 February 2021)

The translucent GGAG:Ce/glass composites are prepared successfully by ball-milling, tableting, and pressureless sintering. The thickness of composites is about 400 μm. The x-ray diffraction (XRD), differential scanning calorimetry (DSC), density of composite materials are measured and discussed systematically. The scanning electron microscopy (SEM) and energy dispersive spectrometer (EDS) elemental mapping are employed to analyze the particle size, the shape of powders, and the distribution of GGAG:Ce particles in the glass matrix, respectively. The decay time, ultraviolet, (UV), x-ray excitation luminescence spectra, and temperature spectra are studied. The results show that the composite materials have high light output, good thermostability, and short decay time. The method adopted in this work is an effective method to reduce the preparation time and cost of the sample. The ultralow afterglow indicates that the composite materials have an opportunity to be used for x-ray detection and imaging.

Keywords: GGAG:Ce, composite material, scintillator, glass matrix, luminescence properties

PACS: 42.70.–a, 78.66.Sq, 81.05.Pj, 81.70.–q **DOI:** 10.1088/1674-1056/abe3ea

1. Introduction

With the development of medical diagnosis, high energy physics, and industry, the demands for scintillators have increased rapidly.[1,2] The scintillation materials with nanosecond fast decay, high density, high efficiency, and stable performance have become a hot spot of research.[3–7] Owing to the excellent scintillation properties,[8–11] such as fast decay (about 50 ns), high light output (6.1×10^4 photons/MeV), and good energy resolution (4.6%@662 keV), $Gd_3Al_3Ga_2O_{12}$:Ce (GGAG:Ce) single crystal and transparent ceramic have tremendous potential applications in many fields such as medical imaging, space detection, security system, high energy physics, *etc*.[12–18] However, the single crystal and transparent ceramic have a shortage of high production cost, long production cycle, and difficulty in large-scale preparation.

Nowadays, due to the great demand for scintillation materials in various fields, many researchers are searching for environmentally friendly and low-cost high-performance scintillation materials. An attractive and novel alternative strategy was found and adopted to prepare scintillation materials, namely "composite scintillation materials," which is produced by embedding the scintillator particles into a transparent matrix.[19] As in previous reports, the composite materials have been well developed and widely used in contemporary material research in recent years, especially for organic transparent materials. The different characteristics of existing materials can be used to produce intelligent materials with original materials' characteristics. As is well known, organic composites, such as quantum-dot organic polymer composites, nanoparticles CeF_3-Oleic acid composites, *etc*. have the advantage of being molded readily, low price and short production cycle.[20,21] Besides, the GGAG:Ce and organic compounds have also been successfully combined to produce high performance organic-inorganic composite films,[22] which can meet the application requirements in imaging fields and radiation detection. However, the organic host still presents many disadvantages, including a lower density, poor radiation hardness for high-energy ray detection, and weaker thermostability. Compared with the organic host, the inorganic glass host material has good temperature stability, radiation hardness, and high density. The researches of porous glass composites or nanoparticle glass composites have been reported and present excellent scintillation properties.[23] The GAGG:Ce/glass composite scintillation material is studied rarely. In the present work, the La_2O_3–SiO_2–Al_2O_3 glass and GGAG:Ce particle are chosen as a composite matrix and phosphor particles, respectively. And then, the GGAG:Ce/glass translucent composite is prepared by ball-milling, tableting, and pressureless sintering method.

In this paper, first, the GAGG:Ce powder is synthesized by the co-precipitation method. Then, the GAGG:Ce phos-

*Project support by the National Natural Science Foundation of China (Grant Nos. 11975220, 51972291, 11575170, and 11605194).
†Corresponding author. E-mail: weiqinhua1985@163.com
‡Corresponding author. E-mail: shs1975@126.com
© 2021 Chinese Physical Society and IOP Publishing Ltd

phor powder is introduced into the extra glass matrix. The homogeneous GAGG:Ce/glass composite powders are obtained by ball milling and sieving. After that, the dense translucent and luminescent ceramic composites are prepared by tableting and sintering. The differential scanning calorimetry (DSC), x-ray diffraction (XRD) patterns, scanning electron microscopy (SEM) microscopic, photoluminescence characteristics, x-ray excited luminescence, and decay time of resulting ceramic samples are analyzed and discussed.

2. Experimental section

2.1. Synthesis of GAGG:Ce nanopowder and glass matrix

The La_2O_3 (purity 99.99%), Gd_2O_3 (purity 99.99%), $Ga(NO_3)_3{\cdot}9H_2O$ (purity 99.99%), were supplied by Fujian Changting Jinlong Rare Earth Co., Ltd, China. The $Ce(NO_3)_3{\cdot}6H_2O$ (purity 99.99%), $Al(NO_3)_3{\cdot}9H_2O$ (purity 99.99%), TEOS (A.R), nitric acid (A.R), ammonium hydroxide (A.R), and ammonium bicarbonate (A.R) were purchased from Sinopharm Chemical Reagent Co. Ltd., China. All chemicals were used directly without any further purification. Distilled water was used in all experiments.

The glass precursor oxide mixture was prepared by a sol–gel technique. The raw materials used in the synthesis of the mix as follows: La and Al-containing solutions were prepared by dissolving La_2O_3, and $Al(NO_3)_3{\cdot}9H_2O$ in nitric acid, Si-solution was prepared by dissolving TEOS in ethanol. The mole ratio of raw materials is $n_{La} : n_{Al} : n_{Si} = 2 : 2 : 6$. The mixed solution was dried at 80 °C and heat-treated at 600 °C for nitrate pyrolysis. The La_2O_3–Al_2O_3–SiO_2 glass was obtained after calcining at 1500 °C for 2 h and then cooled down to room temperature in the furnace as shown in Fig. 1. Finally, the La_2O_3–Al_2O_3–SiO_2 glass was broken into powder for the further experiment. The GGAG:Ce nanopowder was synthesized by chemical co-precipitation method. According to the chemical formula of $Gd_3Al_3Ga_2O_{12}$:Ce, the Gd_2O_3, $Ga(NO_3)_3{\cdot}9H_2O$, $Al(NO_3)_3{\cdot}9H_2O$, and $Ce(NO_3)_3{\cdot}6H_2O$ raw materials were dissolved in 65% concentrated nitric acid. The solution was stirred vigorously and heated. Finally, the concentration of the metal salt mixture was about 0.3 mol/L while the mixture of ammonia and ammonium bicarbonate was about 3 mol/L. The clarified metal salt solution was slowly dripped into the precipitate. The reaction of the endpoint's pH was between 7 and 8. After the titration was completed, the white suspension was stirred for another 30 min before vacuum filtration. The resulting sediment was rinsed with deionized water several times to remove the impurities. Finally, the precursor powder was obtained by drying, grounding and sifting. After that, the precursor was calcined at 950 °C for 2 h, and the GGAG:Ce nanopowder was obtained, as shown in Fig. 1. Additionally, in this process, a weak reducing atmosphere was produced to avoid oxidizing Ce^{3+} into Ce^{4+} by adding the incomplete oxidation of activated carbon.

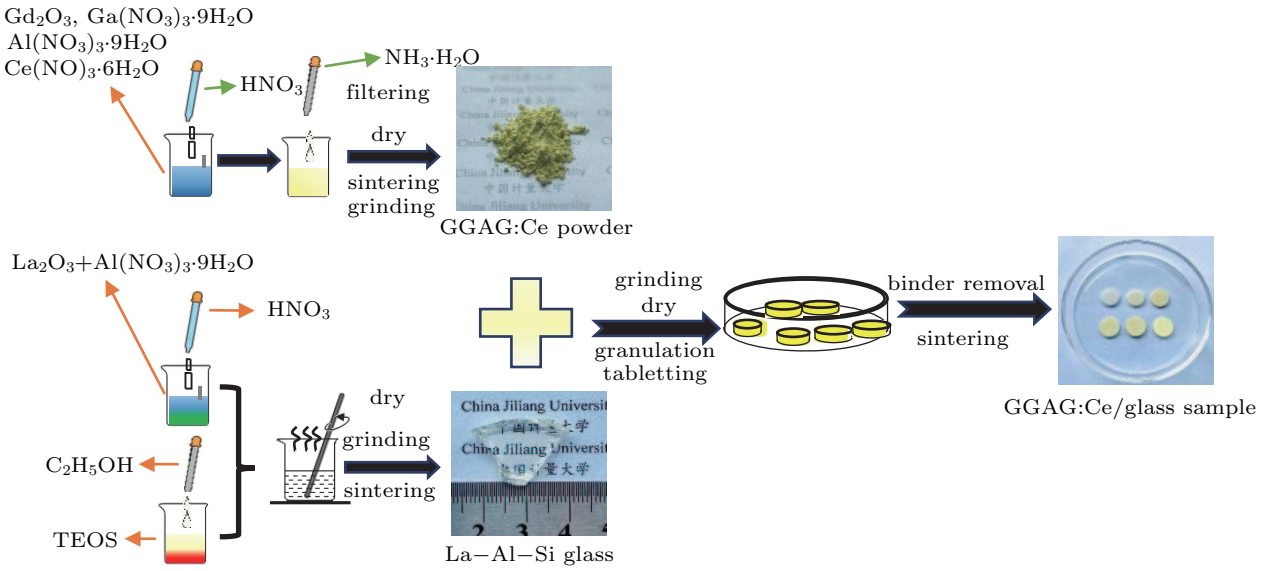


Fig. 1. Preparation flow chart of GGAG:Ce/glass composite material.

2.2. Fabrication of GGAG:Ce/glass composite material

According to the different mass ratios (from 0% to 60%), the GGAG:Ce powder and glass matrix were weighted separately. The GGAG:Ce/glass mixed powder was obtained by balling and sieving. Tableting was performed by using a mold with a diameter of 10 mm. The 8 wt% polyvinyl alcohol was added into the mixed powder as a binder. To eliminate the effect of the binder, the sample was pre-sintering at 550 °C for 10 h in a muffle furnace. Finally, the GGAG:Ce/glass composite material, with a thickness of about 0.4 mm, was produced by sintering at 900 °C for 1 h and polished as shown in Fig. 2. The obtained samples present translucence, and the

transmittance decreased with the GGAG:Ce content increasing. A preparation flow chart of GGAG:Ce/glass composite material is shown in Fig. 1.

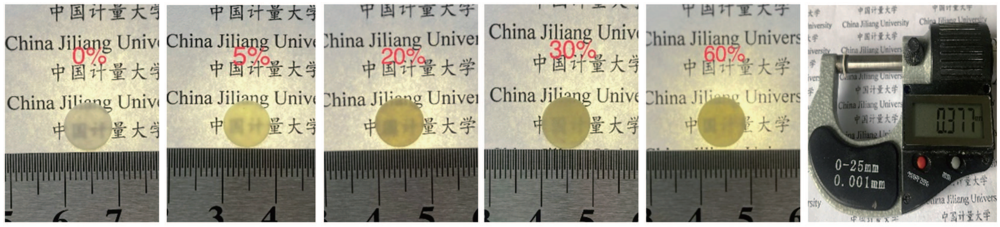
2.3. Material characterization

The crystal structure of powder and ceramic samples were characterized on a Bruker D8 Advance Diffractometer with Cu Ka radiation ($\lambda = 0.1541$ nm). DSC was taken by METTLER with a dry argon atmosphere at the heating rate of 10 °C/min to study the glass transition temperature and crystallizing temperature. The testing temperature was adopted in a range from 25 °C to 1300 °C. The particle size and shape of powders were observed by SEM, Hitachi S-4800). The element distribution of GGAG:Ce particles in La–Al–Si glass matrix was illustrated with energy dispersive spectrometer (EDS). The excitation (PLE) and emission (PL) spectra of composite material under UV light were recorded on a Hitachi F-4600 Spectrometer. The slits for both excitation and emission were both set to be 2.5 nm, and the scan speed was fixed at 240 nm/min. The radioluminescence spectra were also conducted on an x-ray excited luminescence spectrometer (PANalytical Axios). An x-ray tube was used under the condition of $V = 70$ kV and $I = 2$ mA. The decay time of the sample was studied with an FLS920 fluorescence lifetime and steady-state spectrometer. The x-ray-induced afterglow was measured on the x-ray spectrum station DF-7000. Excited with pulsed x-ray of 25-ns pulse width, HAMAMATSU PMT R2059 recorded the data, with the sampling rate being 20 MHz.

3. Results and discussion

Usually, the density of a material is essential for the absorption of high-energy rays. The densities of different components samples are measured by the Archimedes drainage method as shown in Fig. 2. It can be found that the density of the sample increases from 3.63 g/cm^3 to 4.08 g/cm^3 when the concentration of GGAG:Ce increases from 0% to 60%. The composite density is also tunable by substituting La of glass matrix with other rare earth elements (Gd^{3+}, Lu^{3+}), which has potential applications in medical imaging as a scintillator host. The glass matrix's DSC curve is measured as shown in Fig. 3. An endothermic peak and an exothermic peak are observed at 885 °C and 1050 °C, respectively. The endothermic peak of 885 °C can be ascribed to the glass transition, named glass transition temperature (T_g), which means a high glass transition temperature. The exothermic peak of 1050 °C is related to glass crystallizing temperature. Therefore, the sintering temperature of 850 °C–1000 °C is suitable to obtain the GGAG:Ce/glass composite material.

Figure 4 shows the XRD results of the glass matrix, GGAG:Ce powder, and the composite material sample. The XRD standard cards of $Gd_3Ga_3Al_2O_{12}$ (PDF#46-0448) and SiO_2 (PDF#42-0005) are used as a reference. An amorphous diffraction peak, located in a range of 20°–50°, is observed as shown in Fig. 4(a). It indicates that the La–Si–Al glass matrix is obtained successfully. The GGAG:Ce powder sample diffraction peak's position is consistent with that of the standard card by comparing the pattern with standard card data. There is no second phase. Figure 4(b) shows that the diffraction peak positions of GGAG:Ce/glass composite material sample are also consistent with the data of the cards of $Gd_3Ga_3Al_2O_{12}$ (PDF#46-0448) except the impurity peak of 37°. The diffraction peak positions are found to be consistent with the data of the standard card of PDF#42-0005, which can be ascribed to the triclinic structure of SiO_2. Therefore, a small SiO_2 phase is precipitated during sintering at 900 °C, which is lower than the DSC result of 1050 °C. It is possible that the cristobalite phase of SiO_2 crystallizing temperature decreases as the GGAG:Ce powder is added. But, it has no contribution to the luminescence properties under x-ray excitation, which does not affect the composite material's properties, as discussed in Ref. [19].



Sample	0 wt%	5 wt%	20 wt%	30 wt%	60 wt%	GGAG
Density (g/cm^3)	3.63	3.71	3.84	3.86	4.08	6.63

Fig. 2. GGAG:Ce/glass composite samples, thickness, and density.

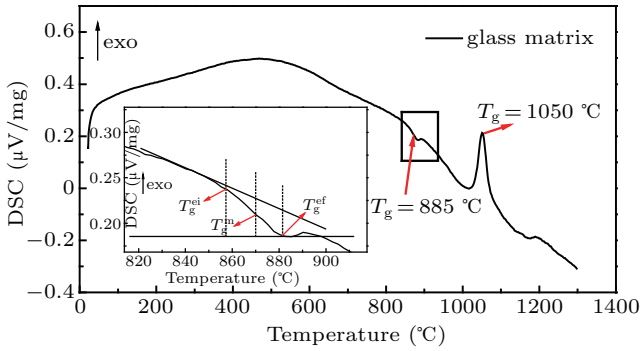


Fig. 3. DSC curve of La–Al–Si glass (25 °C–1300 °C).

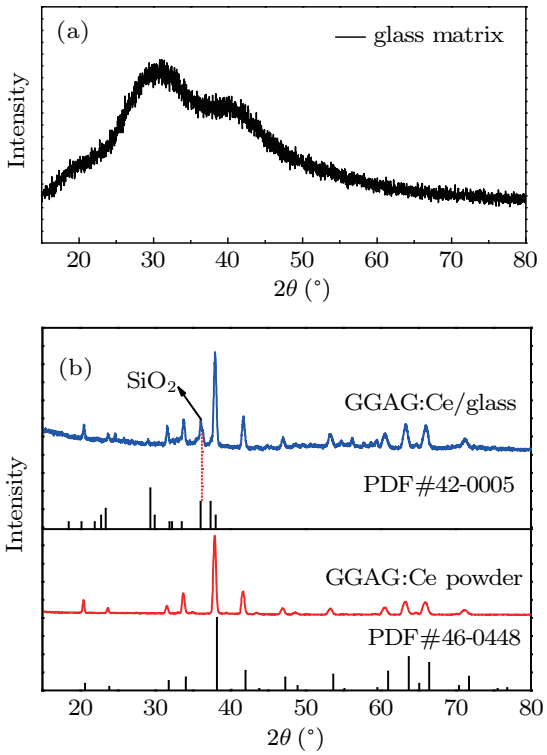


Fig. 4. XRD patterns of (a) glass matrix and (b) GGAG:Ce powder and the composite material sample.

The SEM is a powerful technique to characterize the morphology of GGAG:Ce powder and composite material, while the EDS elemental mapping is used to analyze element distribution in the glass matrix. The results are shown in Figs. 5 and 6. From Fig. 5(a), it can be found that the grain size of GGAG:Ce powder is about 500 nm while the powder is partially agglomerated. The larger particle size of the powder will cause poor dispersion uniformity in the matrix, which ultimately affects the density of the composite material. In this paper, the chemical co-precipitation method is used to prepare the GGAG:Ce powder with smaller particles, which can improve the density of the composite material. Figure 5(b) shows that the composite material has good compactness, but there are still a few pores, which results in a translucent sample. Besides, the uneven distribution of the GGAG:Ce powders in the matrix, leading to the serious scattering and refraction, has an adverse effect on the transparent. The precipitation of SiO_2 in the matrix glass will also affect the transparency of the composite material. In this paper, the sample is prepared by the pressureless sintering method. Usually, to obtain an excellent transmittance, the less residual porosity and higher density of the sample is the key. The use of hot-press sintering (HP), high-temperature isostatic pressing (HIP), and spark plasma sintering (SPS) methods can be used to prepare pore-free or high-density samples. The EDS elemental maps reveal that the sample comprises seven elements (La, Al, Si, Ga, Gd, O, and Ce), which accord with the raw material. Generally speaking, the glass matrix elements of La, Al, Si, and O are evenly distributed, while the GGAG:Ce powder is uniformly dispersed in the glass matrix. However, according to Ga and Gd's element distribution mapping, it found that the GGAG:Ce powder has a slight aggregation.

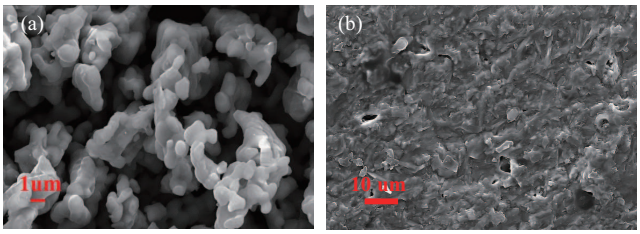


Fig. 5. SEM image of (a) GGAG:Ce powder and (b) composite materials.

The PL and PLE spectra of different samples (λ_{ex} = 450 nm, λ_{em} = 536 nm) are shown in Fig. 7. Figures 7(a) and 7(b) show two excitation peaks, which are located at 350 nm and 450 nm and ascribed to the absorption of Ce^{3+}. Only one main emission peak can be observed for all the samples, which is located at 540 nm. The emission peak can be fitted into two different emission peaks by Gaussian fitting, and assigned to the Ce^{3+} electron transition from the lowest 5d level to $^2F_{5/2}$ and $^2F_{7/2}$ of 4f sublevels as shown in Fig. 7(c). Besides, the luminescence intensity of sample is dependent on GGAG:Ce concentration. The integrated intensity of different PL is shown in Fig. 7(d). The emission intensity first increases and then decreases. The 30% GGAG:Ce/glass sample presents the highest luminescence intensity. Theoretically, the higher content means the stronger luminescence intensity. However, the higher content will lead the powder to disperse unevenly in the matrix. The pore, re-absorption, interface scattering and refraction increase. The transparency decreases while the light loses severely. Compared with the 60% GGAG:Ce sample, the 30% GGAG:Ce sample presents a lower light loss. Therefore, it is reasonable that the 30% of the samples have the strongest luminous intensity.

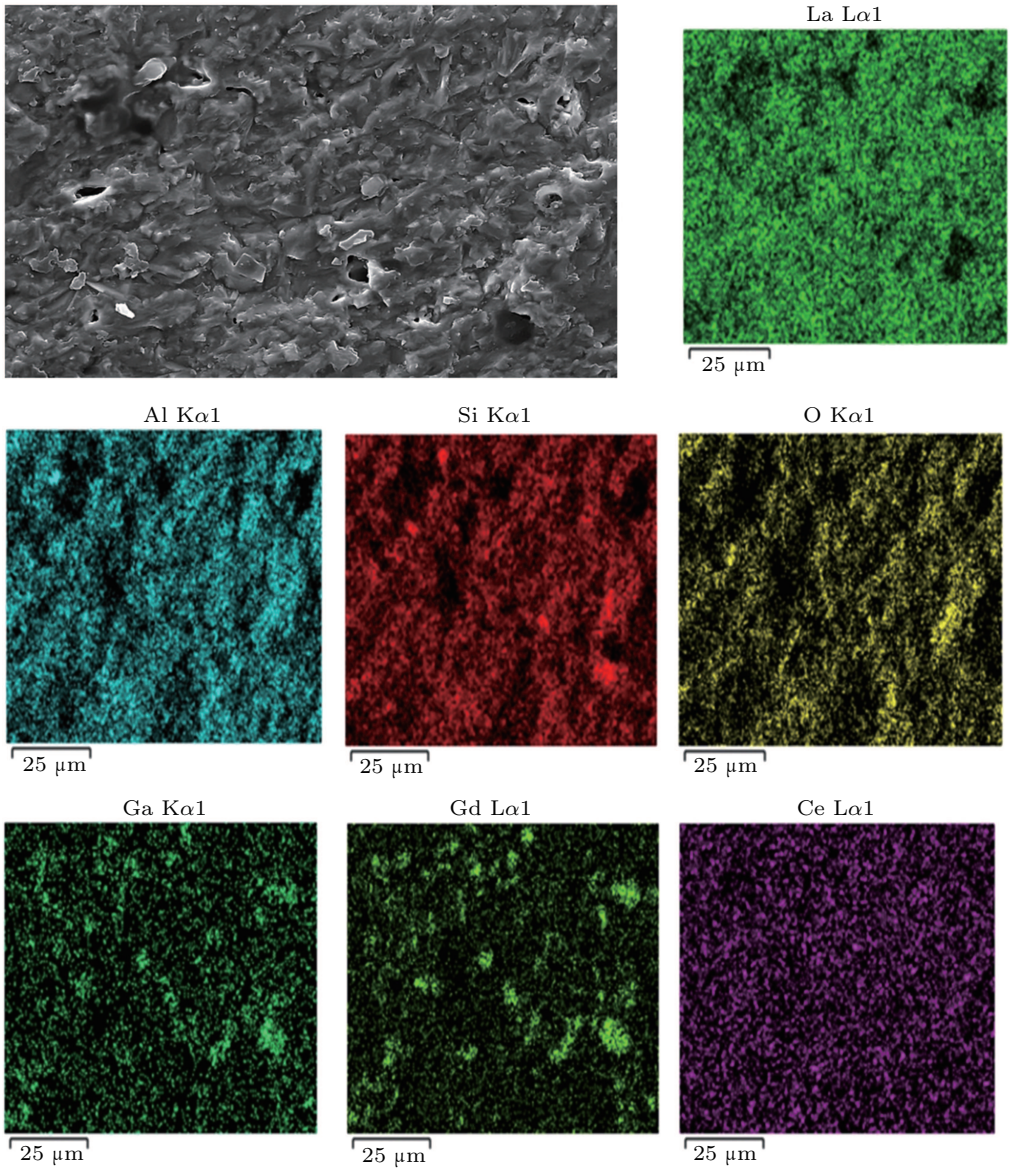


Fig. 6. EDS Elemental mapping of GGAG:Ce/glass composite material.

The emission spectra recorded at room temperature under x-ray excitation for different concentrations of GGAG:Ce/glass samples are presented in Fig. 8. In our experiments, the commercial CsI:Tl crystal is chosen as a reference sample and investigated under the same test conditions to evaluate the luminescence intensity of the GGAG:Ce/glass sample (Fig. 8(a)). The inset of Fig. 8(b) shows the integral intensities of CsI:Tl crystal and GGAG:Ce/glass composite materials with different concentrations. The GGAG:Ce/glass samples present a dominant emission band peak at 520 nm, fitted to two peaks located at 517 nm and 564 nm. This result is in good agreement with that of the PL spectrum under UV radiation. The emission peak is well-matched with the Si-based photodiode.[24] According to the integration values and normalizations of the emission intensity of different samples in XEL spectra, the output of 30% GGAG:Ce/glass is about 33% of the commercial CsI:Tl crystal output while the output of 20% and 60% samples are only 24% and 22% of the commercial CsI:Tl crystal output, respectively. The 30% GGAG:Ce/glass sample presents the highest light output, which is well agreement with the PL result. As the concentration of GGAG:Ce increases, the homogeneity becomes worse and more scattering points and defects are generated, leading to more light to lose. The fluorescence decay time of 30% GGAG:Ce/glass sample at room temperature (RT) with the optimal excitation and emission wavelength ($\lambda_{em} = 536$ nm, $\lambda_{ex} = 450$ nm) is measured and shown in Fig. 8(c). The Decay curves are fitted with a multi-exponential decay function. The fitting formula is as follows:

$$Y = A_1 \exp(-x/\tau_1) + A_2 \exp(-x/\tau_2) + y_0. \quad (1)$$

Here, A_1 and A_2 are the amplitudes, y_0 is the baseline, and τ_1 and τ_2, are the composite material's fluorescence lifetimes. From Eq. (1) and decay curve, the fitting decay time of the

sample is found to be about 8.1 ns (15.9%) and 47.4 ns (82.6%), corresponding to the fast component and slow component, respectively. Compared with the decay time of the GGAG:Ce ceramic sample *i.e.* 4.4 ns and 19.1 ns,[25] the decay time of our sample is reasonable and approximate. The decay time is far superior to that of BGO, NaI (Tl), CsI (Tl) crystals, and film, which meets the requirement for x-ray imaging field's application.[26]

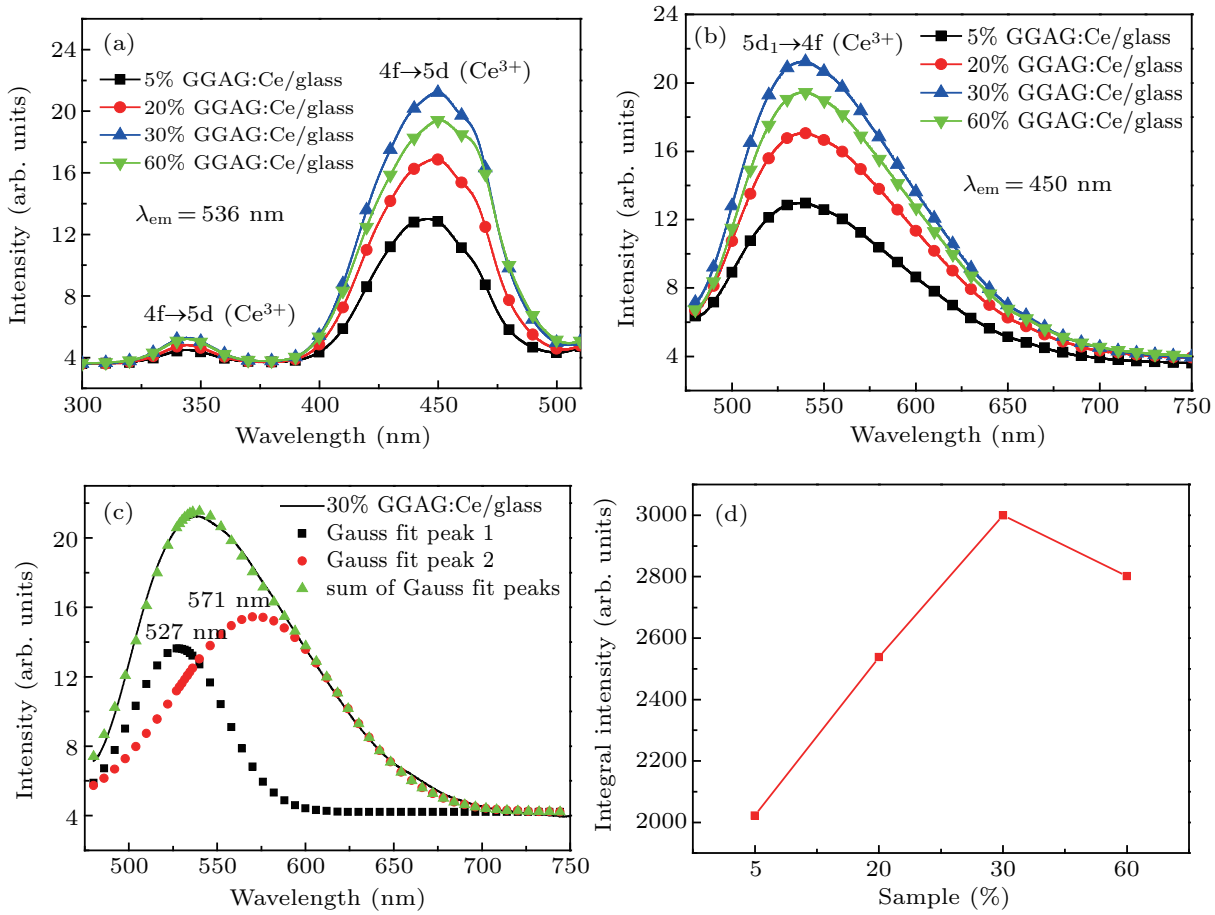


Fig. 7. (a) PLE and (b) PL spectra of GGAG:Ce/glass composite materials ($\lambda_{em} = 536$ nm) with different concentrations. (c) Gaussian fitted (dashed) PL spectrum of GGAG:Ce/glass composite material, and its decomposed components (dotted). (d) Variation of PL integral intensity with concentration of GGAG:Ce/glass composite material.

The x-ray induced afterglow curves of GGAG:Ce/glass composite materials with different concentrations are shown in Fig. 9. The afterglow signals of two samples are dropped by about three orders of magnitude within the first 1 μs. The residual signal of 5%wt GGAG:Ce/glass composite material is 0.2% at 1 μs while that of the 30%wt sample is 0.7% at 1 μs. The afterglow of commercial Gd_2O_2S:Pr (Ce, F) ceramics, used in the X-CT field, is about 10% in a range of 3 μs–6 μs.[27] Therefore, the composite scintillation material has excellent afterglow performance. Meantime, as the concentration increases, the afterglow increases slightly. As is well known, the afterglow is related closely to the defects. It is possible that a higher GGAG:Ce concentration will lead to more defects as discussed in the XEL results. Therefore, it is reasonable that the 5%wt GGAG:Ce/glass sample shows a shorter afterglow. However, more experiments need to be done.

To study the influence of temperature on the luminescence properties of GGAG:Ce composite material, the varying temperature PL spectra of 30% GGAG:Ce/glass sample are measured and shown in Fig. 10 ($\lambda_{ex} = 460$ nm). From Fig. 10(a), it can be seen that when the testing temperature rises from room temperature (RT = 298 K) to 448 K, the luminous intensity of the composite material gradually decreases. As can be seen from the inset in Fig. 10(a), when the temperature rises up to 373 K, the luminous intensity becomes 50% of luminous intensity at room temperature. Nevertheless, when the temperature exceeds 373 K, the emission intensity decreases quickly and the trend of change tends to stabilize after 448 K. This is because the increase in temperature thermodynamically activates the activity of excited state phonons. These activated energies make the excited state levels and ground state energy level overlap, resulting in a non-radiative transition from the excited state to the ground state. The result of the process is that the luminous intensity decreases as temperature increases.

To further explain the relationship between photolumi-

nescence intensity and temperature, the Arrhenius equation is adopted to calculate the activation energy of GGAG:Ce/glass composite materials.[28,29] The equation is shown below.

$$I(T) \approx \frac{I_0}{1 + c\exp\left(\frac{-\Delta E}{KT}\right)}, \tag{2}$$

where $I(T)$ corresponds to the luminous intensity at temperature T, I_0 is the initial intensity, c is the frequency factor, ΔE is the thermal quenching activation energy, and k is the Boltzmann constant ($k = 8.629 \times 10^{-5}$ eV/K). The thermal quenching activation energy of GGAG:Ce/glass composite is presented in Fig. 10(b). Through linear fitting, the activation energy of GGAG:Ce/glass composite material is about 0.401 eV, which is close to the activation energy of GGAG:Ce ceramics.[30] It shows that the composite material has good thermal stability. As discussed above, the GGAG:Ce/glass composite material presents good light output and ultralow afterglow under x-ray radiation. It indicates that the material is a sensitive scintillator used in actual x-ray inspection applications, such as computer tomography.

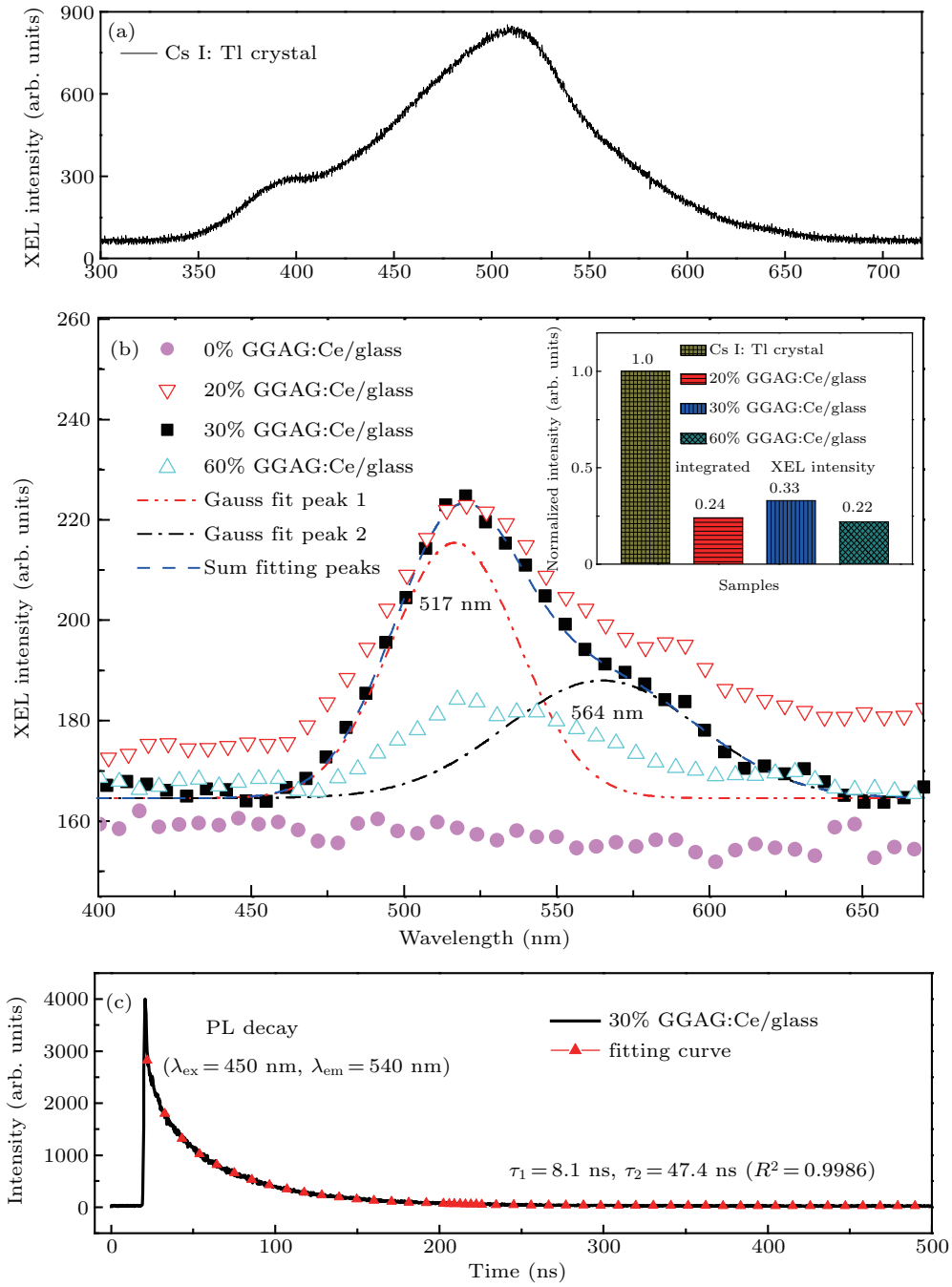


Fig. 8. (a) X-ray excited luminescence of CsI:Tl crystal, (b) x-ray excited luminescence intensities *versus* wavelength of GGAG:Ce/glass composite materials with different concentrations and the fitting results of 30%wt GGAG:Ce/glass composite material, with inset showing integral intensity of CsI:Tl crystal and GGAG:Ce/glass composite material with different concentrations. (c) The fluorescence decay curve of GGAG:Ce/glass composite.

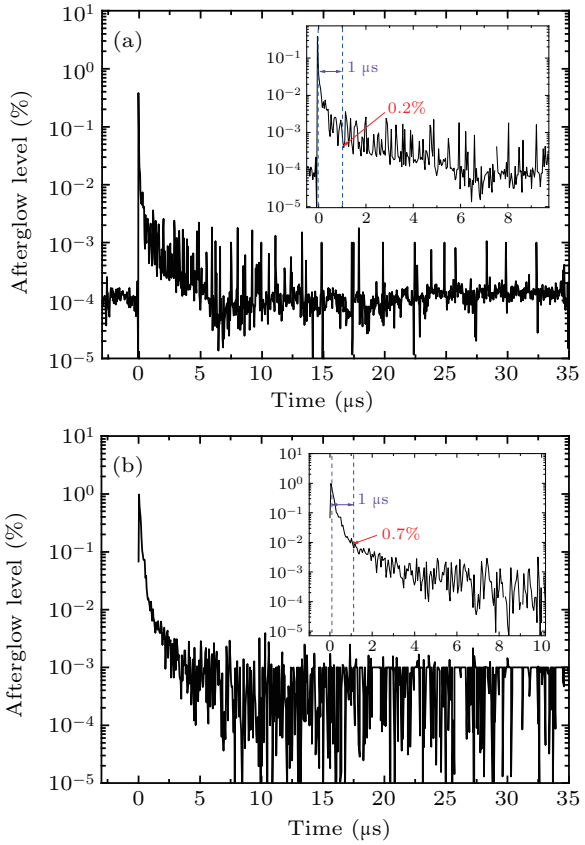


Fig. 9. The x-ray-induced afterglow profile of (a) 5%GGAG:Ce/glass composite material and (b) 30%GGAG:Ce/glass composite material.

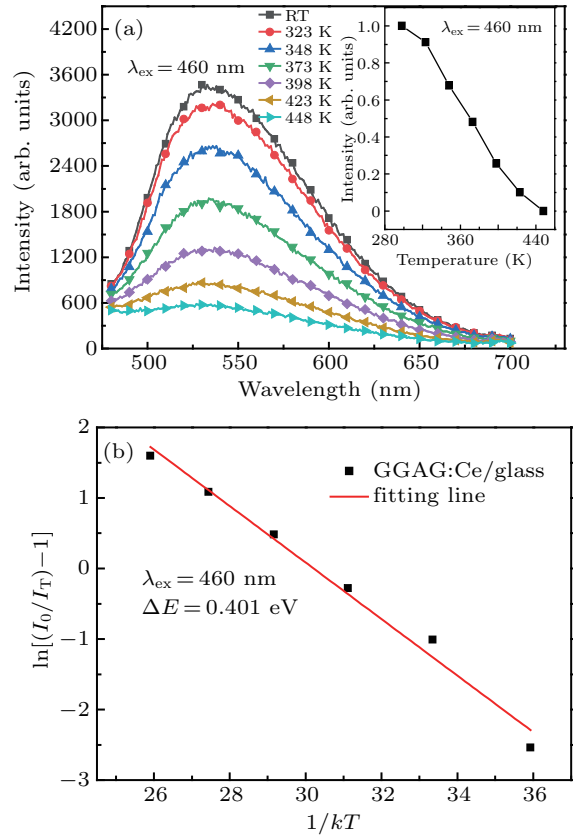


Fig. 10. (a) Variable temperature emission spectra of GGAG:Ce/glass composite material, with inset showing normalized relationship between luminous intensity and temperature; (b) thermal activation energy of GGAG:Ce/glass composite material.

4. Conclusions

In this work, the GGAG:Ce/glass translucent composite has been successfully fabricated with GGAG:Ce phosphor embedded in the glass matrix by balling and pressureless sintering at a temperature of 900 °C. The required GGAG:Ce/glass composite powders are prepared by a chemical coprecipitation and sol–gel method, respectively. The GGAG:Ce particles are uniformly distributed in the glass matrix. The sample's density can be tuned from 3.63 g/cm^3 to 4.08 g/cm^3 by adjusting the concentration of GGAG:Ce powder and the glass matrix. The maximum emission peak of the GGAG:Ce/glass composite is located at 540 nm under x-ray excitation, corresponding to the electron transition from the 5d level to 4f level of Ce^{3+}. The decay times of the GGAG:Ce/glass composite are found to be about 8.1 ns (15.9%) and 47.4 ns (82.6%) by fitting. Its scintillation yield is approximately 1/3 times of the commercial CsI:Tl crystal while it has a low afterglow in a range of 0.2%–0.7% at 1 μs under x-ray radiation. The GGAG:Ce/glass composite material also has good thermal stability, and the activation energy is about 0.401 eV. The composite material has the advantages of the simple preparation process and low cost, thus has a potential application in the x-ray imaging field.

Acknowledgment

The authors thank Prof. Yuntao Wu of Shanghai Institute of Ceramic and Prof. Fan Yang of Nankai University for their testing support.

References

[1] Nikl M and Yoshikawa A 2015 *Adv. Opt. Mater.* **3** 463
[2] Fasoli M, Vedda A, Nikl M, Jiang C, Uberuaga B P, Andersson D A, Mcclellan K J, and Stanek C R 2011 *Phys. Rev. B* **84** 081102
[3] Burger A, Rowe E, Groza M, Figueroa K M, Cherepy N J, Beck P R, Hunter S and Payne S A 2015 *Appl. Phys. Lett.* **107** 143505
[4] Wu Y, Koschan M, Foster C and Melcher C L 2019 *Cryst. Growth Des.* **19** 4081
[5] Foster C, Wu Y, Stand L, Koschan M and Melcher C L 2019 *J. Lumin.* **216** 116751
[6] Wei Q, Shi H, Zhou Z, Liu G, Chen Z, Qin L and Liu Q 2017 *J. Mater. Chem. C* **5** 1443
[7] Wu Y, Peng J, Rutstrom D, Koschan M, Foster C and Melcher C L 2019 *ACS Appl. Mater. Interfaces* **11** 8194
[8] Kamada K, Yanagida T, Endo T, Tsutumi K, Usuki Y, Nikl M, Fujimoto Y, Fukabori A and Yoshikawa A 2012 *J. Cryst. Growth* **352** 88
[9] Sibczynski P, Iwanowska-Hanke J, Moszyński M, Swiderski L, Szawłowski M, Grodzicka M, Szczęśniak T, Kamada K and Yoshikawa A 2015 *Nucl. Instrum. Methods Phys. Res., Sect. A* **772** 112
[10] Kanai T, Satoh M, and Miura I 2013 *Int. J. Appl. Ceram. Technol.* **10** E1
[11] Drozdowski W, Witkowski M E, Solarz P, Głuchowski P, Głowacki M and Brylew K 2018 *Opt. Mater.* **79** 227
[12] Blasse G 1994 *Chem. Mater.* **6** 1465
[13] Greskovich C D, Cusano D, Hoffman D and Riedner R J 1992 *Am. Ceram. Soc. Bull.* **71** 1120
[14] Yanagida T, Kamada K, Fujimoto Y, Yagi H and Yanagitani T 2013 *Adv. Opt. Mater.* **35** 2480
[15] Luo Z, Jiang H, Jiang J and Mao R 2015 *Ceram. Int.* **41** 873
[16] Chen J, Shi Y, Feng T and Shi J 2004 *J. Chin. Ceram. Soc.* **32** 868 (in Chinese)

[17] Philip O, Gunow G, Shestakova I, Berheide M, Durner E, Stoller C and Cherepy N 2015 *IEEE Nuclear Science Symposium and Medical Imaging Conference (NSS/MIC)*, 31 October–7 November 2015, San Diego, CA, USA, p. 1
[18] Chen X, Qin H, Wang X, Yang C, Jiang J and Jiang H 2016 *J. Eur. Ceram. Soc.* **36** 2587
[19] Wei Q, Zhuang J, Liu G, Zhou Z, Yang H, Wang J and Liu Q 2014 *RSC Adv.* **4** 33819
[20] Feller R K, Purdy G M, Ortiz-Acosta D, Stange S, Li A, McKigney E A, Esch E I, Muenchausen R E, Gilbertson R and Bacrania M J 2011 *J. Mater. Chem.* **21** 5716
[21] Lawrence W G, Thacker S, Palamakumbura S, Riley K J and Nagarkar V V 2012 *IEEE Trans. Nucl. Sci.* **59** 215
[22] Sen S, Tyagi M, Sharma K, Sarkar P S, Sarkar S, Basak C B, Pitale S, Ghosh M and Gadkari S C 2017 *ACS Appl. Mater. Interfaces* **9** 37310
[23] Letant S E and Wang T F 2006 *Nano Lett.* **6** 2877
[24] El-Amir A A, Ohsawa T, Nabatame T, Ohi A, Wada Y, Nakamura M, Fu X, Shimamura K and Ohashi N 2019 *Mater. Sci. Semicond. Process.* **91** 222
[25] Ye Y 2017 *Fabrication and Properties of Ce:GGAG Scintillator Ceramics*, Master Dissertation (Xuzhou: Jiangsu Normal University) (in Chinese)
[26] van Eijk C W E 2003 *Nucl. Instrum. Methods Phys. Res., Sect. A* **509** 17
[27] Yoshida M, Nakagawa M, Fujii H, Kawaguchi F, Yamada H, Ito Y, Takeuchi H Hayakawa T and Tsukuda Y 1988 *Jpn. J. Appl. Phys.* **27** L1572
[28] Wei Q, Liu Y, Miao Y T, Li Y, Shi H and Qin L 2018 *J. Lumin.* **194** 610
[29] Bhushan S and Chukichev M V 1988 *J. Mater. Sci.* **7** 319
[30] Liu P, Liu Y, Wang L, Qiao J, Huang P, Shi Q, Tian Y, Jiang H and Jiang J 2018 *J. Alloys Compd.* **731** 389